Journal of Materials Chemistry A

Regulating the growth of aluminum electrodeposits: towards anode-free Al batteries

Journal:	*Journal of Materials Chemistry A*
Manuscript ID	TA-COM-08-2020-008505.R1
Article Type:	Communication
Date Submitted by the Author:	20-Sep-2020
Complete List of Authors:	Zhao, Qing; Cornell University, Chemical and Biomolecular Engineering Zheng, Jingxu; Cornell University, Deng, Yue; Cornell University Archer, Lynden; Cornell University, Chemical and Biomolecular Engineering

Journal Name

ARTICLE

Regulating the growth of aluminum electrodeposits: towards anode-free Al batteries

Qing Zhao[a†], Jingxu Zheng[b†], Yue Deng[b], Lynden Archer[a,b*]

Received 00th January 20xx,
Accepted 00th January 20xx

DOI: 10.1039/x0xx00000x

www.rsc.org/

The high earth abundance and large specific capacity of aluminum Al on either a volume (8040 mAh cm^{-3}) or mass (2980 mAh g^{-1}) basis continues to drive interest in electrochemical cells that utilize metallic Al as the anode. At practical anode capacities uneven, non-planar deposition of Al during battery recharge combine with the high Young's modulus (E_{Al}=70Ga) of the metal to limit the electrode lifetime in all known electrolytes. Here we study the effect of a thin, textured coating composed of two-dimensional gold nanosheets with strong diffraction from (111) facets and low lattice mismatch for Al, as a substrate for regulating the Al electrodeposit morphology. We report that these coatings are not only effective in preventing Al deposition in non-planar morphologies, but have a large beneficial effect on the reversibility of Al electrodes. In Al plating/stripping studies, the textured Au coatings sustain stable cell operations for 500 cycles or more with a high Coulombic efficiency of over 99%. Full cell Al batteries composed of the Au nanosheets as the anode substrate and graphene as cathode are reported to exhibit capacity retention of 80% after 1000 charge-discharge cycles, and 74% at the 2000th cycle, exceeding the lifetimes (~200 cycles) of comparable Al batteries in which a standard stainless steel material is used as the anode substrate. Our results demonstrate that through rational design of the substrate for Al deposition, both the electrodeposit morphology and cycle life of Al-based batteries can be markedly improved.

Introduction

Lightweight (Li^+, Na^+) and multivalent (Mg^{2+}, Al^{3+}) metal-ion batteries have been widely studied over the last half century — during a period when application of Li-ion batteries has brought incomparable convenience in essentially every aspect of daily life.[1-4] In recent years, aluminum (Al) based batteries have attracted attention due to the high theoretical specific capacity of the anode —both by weight (2980 mAh g^{-1}) and volume (8040 mAh cm^{-3}), in comparison with lithium metal (3862mAh g^{-1}, 2062 mAh cm^{-3}).[5-10] Al is known to be passivated by a dense oxidation layer composed primarily of Al_2O_3, which can stabilize the Al metal in contact with atmospheric oxygen and moisture, but which poses a formidable barrier to oxidation of Al to form mobile Al^{3+} in the majority of battery electrolytes.[11] Most organic electrolytes that show promise in batteries employing alkali metal (*e.g.,* Li, Na) anodes sustain impractically sluggish electrode kinetics in Al batteries.[3, 12-16]

Multiple previous studies have shown that ionic liquid (IL)-based electrolytes, for example, the eutectic formed by mixing $AlCl_3$ and 1-Ethyl-3-methylimidazolium chloride ([EMIm]Cl), are able to overcome these barriers and to support efficient plating and stripping of Al metal electrodes.[17] Various materials,[18] including carbon chemistries,[6, 19-21] sulfur or sulfides,[22-27] iodine,[28] tellurium,[29] metal oxides,[30-33] MXene,[34] organic compounds[35, 36] have likewise been reported to sustain reversible cycling of Al in IL-based electrolytes. Among these Al battery chemistries, cells in which a metallic Al anode is paired with graphite or few layer graphene as cathode have demonstrated exceptional reversibility, in one case reaching over 250,000 charge-discharge cycles.[18] Considering the inherently low cost of the anode and cathode in such cells, Al cells based on any of these chemistries hold promise for dramatically reducing the cost of energy storage — perhaps even to the point where on an amortized/lifetime basis, the cost of electrical energy storage becomes irrelevant in comparison to other costs associated with electric power generation or conversion using renewable solar or wind resources. Realization of such a storage platform on practical scales would be of interest for stationary as well as mobile applications where the cost of electrical energy storage continues to present a barrier to consumer acceptance.

In principle, Al//Graphite (or graphene) cells based on IL electrolytes are dual-ion batteries (**Figure 1a**). In such cells the Al metal anode acts as the counter electrode and does not contribute to the overall energy stored. All energy is generated as a result of redox reactions between soluble species in the electrolytes.[37,38] In an acidic IL-based electrolyte (*e.g.*, $AlCl_3$:[EMIm]Cl > 1), $AlCl_4^-$ and $Al_2Cl_7^-$ are the two principal

[a] Robert Frederick Smith School of Chemical and Biomolecular Engineering, Cornell University, Ithaca, New York 14853, United States..
[b] .Department of Materials Science and Engineering, Cornell University, Ithaca, New York 14853, United States
† These authors contribute equally.
Electronic Supplementary Information (ESI) available: [details of any supplementary information available should be included here]. See DOI: 10.1039/x0xx00000x

anions in the electrolytes. In the charging process, $Al_2Cl_7^-$ is reduced at the anode to form Al and $AlCl_4^-$, and $AlCl_4^-$ is thought to intercalate into the layered graphite anode. The discharging process occurs reversibly. Compared with dual-ion Li, Na, or K batteries (**Figure 1b**) that largely consume cation (Li^+) and anion (PF_6^-) in the charging process, the electrode reactions in such a dual-ion Al battery would not reduce the overall concentration of ions in the electrolyte (see overall reaction in **Figure 1c**). The charging process will stop when all $Al_2Cl_7^-$ is transferred to $AlCl_4^-$ and the electrolytes become neutral ($AlCl_3$: [EMIm]Cl = 1). In this situation, the ionic-conductivity may even rise above that of the original acidic melt (> 10mS/cm at room temperature), during the battery cycling. As a comparison, the charging process of a dual-ion Li battery will continuously consume Li^+ and PF_6^-, which makes the ion transport sluggish near the end of charge. Meanwhile, due to the high concentration of IL-based electrolyte, the specific capacity of dual-ion Al batteries is higher than dual-ion Li batteries. In addition, the cycle life of the former (up to quarter-million cycles[18]) also exceeds that of the later (hundreds of cycles[39,40]) due to the fundamental stability of the IL-based electrolytes.

While the dual-ion Al battery concept is known, the excellent performances characteristics reported thus far are typically based on cells in which a thin, low-capacity graphite/graphene cathode is employed. [2,9,19] We note that the areal capacity of Al for each cycle in such cells is less than 0.2mAh/cm^2. This small amount capacity along with the effectively infinite electrolyte volume (~100µl) available in the cells results in a negligible energy density, when considering the overall mass. In addition, the propensity of the Al anode to deposit in non-planar configurations, which can reduce the lifetime of a battery cell by short-circuiting the electrodes, is known but typically ignored in the literature because the effect of common mitigation strategies (*e.g.*, multiple layers of separator), [6] on overall energy density is normally not studied. Additionally, the very small amount of Al deposited upon charging contemporary Al//graphite cells means that it is practically impossible for the non-planar deposits to become large enough to bridge the inter-electrode spacing, which reduces the risk of premature battery failure by dendrite-induced short circuits. When higher amount of Al is deposited for each cycle, the high Young's modulus (E_{Al}=70Ga), in comparison to Li (E_{Li}=5Ga), indicates that the search for effective, practical approaches for preventing cell failure by dendritic growth of Al is actually far more challenging than the analogous search in the Li metal battery field. Indeed, some of the most promising approaches proposed for Li, such as mechanically blocking the non-planar structures from growing using solid-state electrolytes, would not work for the inherently stronger and multi-valent Al.

A fundamental strategy for overcoming challenges with non-planar Al electrodeposition at the anode could be to utilize a thin, epitaxial coating analogous to what we reported recently for Zn to regulate its electrodeposition, and to form compact, planar structures.[41,42] Specifically, if a substrate can be identified with a lattice misfit less than 15% for the fresh Al electrodeposit phase, the new phase is hypothesized to exhibit a correlated growth orientation in relation to the substrate.[41] Al with face-centered cubic (FCC) crystal structure shares a lot of similarities with other FCC metals, including Au and Ag. For example, the lattice misfit between gold (Au) and Al is only 0.7%, indicating Au is a potential substrate to epitaxially regulate the growth of Al. Additionally, in comparison to the typically used stainless steel substrate, which is easily corroded by IL-based electrolytes[43, 44], Au offers superior corrosion resistance. Moreover, synthesis of nanostructured Au materials with well-defined exposed crystallographic facets has received intense interest for decades, particularly as catalysts and for electronics.[45, 46] Methods for synthesizing crystalline, two-dimensional (2-D) Au nanosheets with high-aspect-ratio and which selectively expose (111) planes as the major lattice facet have also been reported by many authors.[46, 47] Previous calculations have shown that the (111) facet of Al has lower surface energy (0.96 J/m^2) compared with other facets.[48] Thus, we hypothesize that a substrate composed of organized Au nanosheets with strong diffraction from these (111) facets should facilitate more compact electrodeposition of Al.

Herein, we design substrates for Al anodes based on 2-D Au nanosheets that preferentially expose (111) facets. We subsequently use these substrates to create Al metal free dual ion IL-based Al batteries with high levels of reversibility. We begin by investigating the morphology of Al electrodeposits at these substrates and, consistent with our hypothesis, find that Al deposits in the form of small, uniform particles with average size below 250nm. This could be compared with the large, discrete structures formed on a stainless-steel electrode. Direct visualization studies show, further, that whereas Al deposits on the structured Au-coated substrates are compact and decidedly non-dendritic, even at a high current density of 15mA/cm^2, the analogous deposition on stainless steel is obviously non-planar and dendritic, explaining literature reports that dendrite-induced short circuiting is a common failure mode for such cells. Significantly, we also find that Al deposited on the Au-based substrate exhibit extremely high (>99%) plating/stripping efficiencies in long-term cycling experiments, without failing by short-circuits. As a final, rigorous test of the utility of the electrode design, we create dual-ion Al batteries applying graphene cathode and an Au coating as the anode and demonstrate long-term cycling stability for 2000 cycles with capacity retention exceeding 74%.

Journal Name

ARTICLE

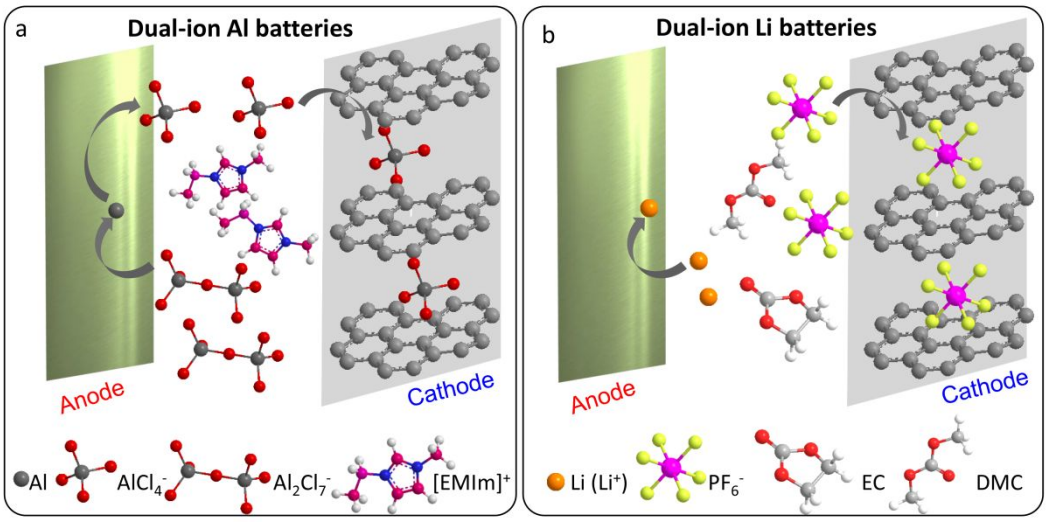

c

	Dual-ion Al batteries	Dual-ion Li batteries
Components	$AlCl_4^-$, $Al_2Cl_7^-$, $EMIm^+$	Li^+, PF_6^-, EC, DMC
Reaction	Anode: $4Al_2Cl_7^- + 3e^- \underset{\text{Discharge}}{\overset{\text{Charge}}{\rightleftharpoons}} 7AlCl_4^- + Al$ Cathode: $3AlCl_4^- + C_n - 3e^- \underset{\text{Discharge}}{\overset{\text{Charge}}{\rightleftharpoons}} C_n[AlCl_4]_3$ Overall: $4Al_2Cl_7^- + C_n \underset{\text{Discharge}}{\overset{\text{Charge}}{\rightleftharpoons}} C_n[AlCl_4]_3 + 4AlCl_4^- + Al$	Anode: $Li^+ + e^- \underset{\text{Discharge}}{\overset{\text{Charge}}{\rightleftharpoons}} Li$ Cathode: $PF_6^- + C_n - e^- \underset{\text{Discharge}}{\overset{\text{Charge}}{\rightleftharpoons}} C_n[PF_6]$ Overall: $Li^+ + PF_6^- + C_n \underset{\text{Discharge}}{\overset{\text{Charge}}{\rightleftharpoons}} C_n[PF_6] + Li$
Electrolytes	Before charge: $AlCl_3$:[EMIm]Cl> 1:1 After charge: $AlCl_3$:[EMIm]Cl= 1:1	Before charge: xM $LiPF_6$ EC/DMC After charge: <xM $LiPF_6$ EC/DMC
Capacity	By cathode: 120mAh/g Overall capacity: 23mAh/g ($AlCl_3$:[EMIm]Cl= 1.5:1) 35mAh/g ($AlCl_3$:[EMIm]Cl = 2:1)	By cathode: 100mAh/g Overall capacity: 10 mAh/g (1M $LiPF_6$ to 0.5M $LiPF_6$) 24 mAh/g (2M $LiPF_6$ to 0.5M $LiPF_6$)
Ion conductivity	$AlCl_3$:[EMIm]Cl = 2:1 (~13mS/cm) 1.5:1 (~17mS/cm) 1:1 (~19mS/cm)	$LiPF_6$ EC/DMC: 2M (~6mS/cm) 1M (~9.5mS /cm) 0.5M (~7.8mS/cm) 0.2M (4.5mS/cm)

Fig. 1. Comparisons of dual-ion Al batteries and dual-ion Li batteries. schematic diagram of a) dual-ion Al and b) dual-ion Li batteries. c) Detailed comparisons of two battery systems. References for specific capacity by cathode,[18, 39] references for ion conductivity.[49-51]

Experimental

Synthesis of Au nanosheet:

Au nanosheet is synthesized according to previous report[47]. In brief, 222mg PVP with molecular weight of 40K (Sigma-Aldrich) was first dissolved in 20ml ethylene glycol (Sigma-Aldrich). Then 0.4ml aqueous $HAuCl_4$ (Sigma-Aldrich) (250mM) solution was added. Then solution was then transferred to a 50ml hydrothermal reactor and heat at 120°C in oven for 12 hours. After reaction, the products were centrifuged by ethanol for 3 times. 2ml 1-butanol was then added to the products and dispersed by ultrasound to generate a uniform solution.[46] The solution was then dipped on the stainless steel (SS) and was quickly dried in vacuum oven at 80 °C to fabricate the Au nanosheet coated SS (Au-SS). The loading of Au nanosheet on SS is 1~2mg/cm^2.

Materials characterization:

Optical visualizations of Al deposition were recorded by OLYMPUS DP 80. Leo 1550 Keck Field Emission Scanning

Electron Microscopy with Bruker EDX detector was used to obtain SEM images and EDX mapping. Galvanostatic tests of electrochemical cells were performed using Neware battery tester at room temperature. The XRD pattern of Au nanosheet was taken on Rigaku X-Ray diffractometer.

Study of Al electrochemical deposition:

$AlCl_3$ (99.99%; Sigma-Aldrich) -[EMIm]Cl(>95%; Sigma-Aldrich) with molar ratio of 1.5:1 are used for the study of electrochemical deposition. The electrolyte was synthesized by adding $AlCl_3$ into [EMIm]Cl slowly with continuous stirring until forming clear solution. All the experiments were conducted in Ar-filled glove box (Inert Inc.). In order to obtain the SEM image of Al deposition, coin cells with PTFE O-ring (Thickness: 0.78mm, Diameter: 6.35mm) as separator were assembled. The coin cells were assembled with the order of Al anode, O-ring filled with electrolytes, stainless steel (SS) spacer (or Au-SS spacer), and spring. The assembled electrochemical cells were discharged at current density of 1mA/cm^2 for 10mins in order to deposit Al on the SS or Au-SS spacer. The cells were disassembled in glovebox, and the spacers were washed by anhydrous tetrahydrofuran (THF) before SEM test. In situ visualization test of the electrochemical deposition of Al was performed using a converted cuvette cell.[52] One piece Al anode, and one piece SS or Au-SS (counter electrode) were put into cuvette in parallel.

Graphene (G) cathode preparation and Battery assembly:

Graphene cathodes were prepared using graphene dispersion in water (Dia:1-3μm) (ACS MATERIALS®). The solution were dipped on the substrate of carbon cloth (Fuel Cell Store) and dried in the vacuum oven. The G-cathode was obtained after drying at 100 °C for 12 hours. The loading of G on carbon cloth was 3~5mg/cm^2. Glass fiber (GF/D Whatman™) was used as separator. The amount of electrolyte was 80-100μl. Additional thin PTFE O-rings and carbon fiber spacers were used to cover the edge of electrodes, which were applied to avoid the corrosion of batteries for long-term cycling.

Discussions on dual-ion Al batteries and dual-ion Li batteries:

The highest specific capacity of Al//Graphite (graphene) batteries are obtained from literature (120mAh/g).[18] The practical capacity is calculated by the formula of $\frac{\boldsymbol{specific\ capacity\ of\ cathode} \times \boldsymbol{mass\ of\ cathode}}{\boldsymbol{mass\ of\ cathode} + \boldsymbol{mass\ of\ electrolytes}}$, because the mass of anode can be neglected by the ultrathin substrate (for example, Au nanosheet in this work). 1 mole electrolyte ($AlCl_3$: [EMIm]Cl=1.5:1) contains 0.6 mol $AlCl_3$ and 0.4 mol [EMIm]Cl with a total mass of 138.7 g. After dissociation, the electrolyte contains 0.2 mol $AlCl_4^-$, 0.2 mol $Al_2Cl_7^-$ and 0.4 mol $EMIm^+$. According to the overall reaction in Fig. 1c, all $Al_2Cl_7^-$ will be consumed to generate the same amount of $AlCl_4^-$. Here, after full charge, the electrolyte contains 0.4 mol $AlCl_4^-$ and 0.4 mol $EMIm^+$. The electron transfer after full charging is 0.15 mol, corresponding to an electrical energy of 4 Ah with consumption of 33.3 g cathode. Therefore, the overall capacity is 23 mAh/g ($\frac{\mathbf{4 \times 1000\ mAh}}{\mathbf{138.7g + 33.3g}}$). For 1 mole electrolyte with high ratio of $AlCl_3$ ($AlCl_3$: [EMIm]Cl=2:1, mass: 137.8 g). The electrolyte contains $\frac{1}{3}$ mol $Al_2Cl_7^-$ and $\frac{1}{3}$ mol $EMIm^+$. After charge, all $Al_2Cl_7^-$ transfers to $AlCl_4^-$ and electrolyte becomes $\frac{1}{3}$ mol $AlCl_4^-$ and $\frac{1}{3}$ mol $EMIm^+$. The electron transfer after full charging is 0.25 mole, corresponding to an electrical energy of 6.7 Ah with consumption of 55.8 g cathode. Therefore, the overall capacity is 35 mAh/g ($\frac{\mathbf{6.7 \times 1000\ mAh}}{\mathbf{137.8g + 55.8g}}$). The specific capacity of dual-ion Li batteries is calculated by the same method, in which the specific capacity by cathode is set as 100mAh/g [37]. The electrolytes of 1M $LiPF_6$ and 2M $LiPF_6$ in EC/DMC are used. The reaction is defined to be terminated when the concentration of electrolytes are reduced to 0.5M with the consideration of ion transport.

Results and discussions

As shown in **Figure 2b** and **Figure S1**, thin Au nanosheets with sizes in the range of 10-20 μm are synthesized. The standard XRD profiles show that Al and Au are FCC crystal structure with same space group of Fm-3m (**Figure 2a**). The XRD profile for commercial Al foil fits well with standard card, exhibiting two major diffraction peaks of (111) and (200). The synthesized Au nanosheets (blue lines in Figure 2a) exhibit a strong diffraction associated of Au (111) with negligible diffraction of (200). This strong anisotropy is largely a result of the large size and anisotropy of the synthesized Au sheets, which readily promotes their strong alignment in a highly textured planar configuration.

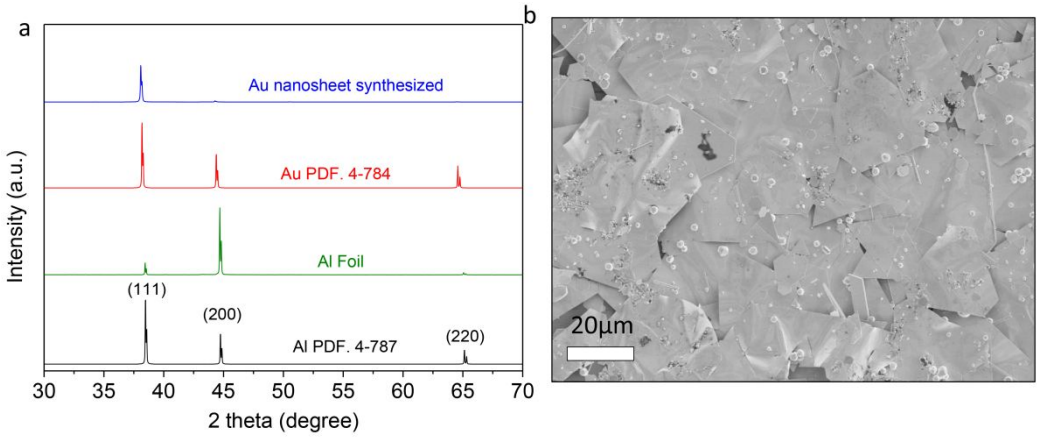

Fig. 2: (a) XRD profiles and (b) SEM image of synthesized Au nanosheets

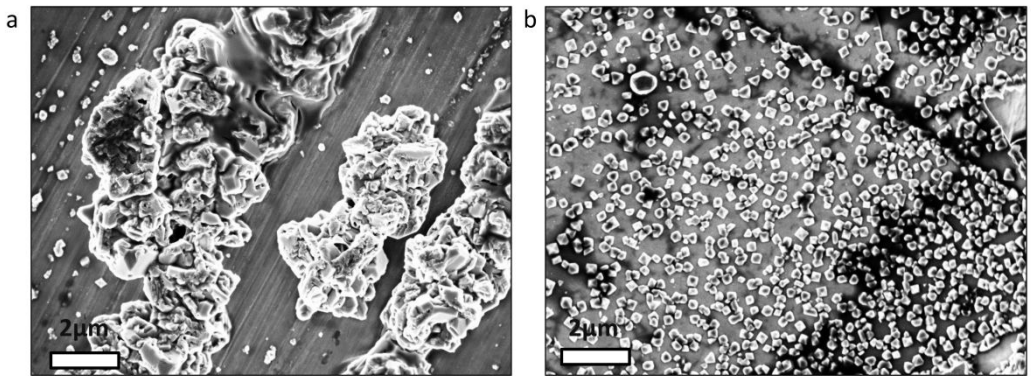

Fig. 3: SEM images of electrodeposited Al on a) stainless steel and b) Au nanosheets. Al is deposited on SS and Au in pressure-free Al//SS and Al//Au-SS electrochemical cells. The current density is 1mA/cm^2.

The typical morphology of Al deposited on SS is seen to be an ensemble of randomly distributed large particle clusters (**Figure 3a**) that form a heterogeneous landscape on the substrate. Subsequent deposition of Al is templated by these structures and leads to accumulation of even bigger, more heterogeneous structures. Considering the high Young's modulus of Al, the uneven deposition of Al provides obvious risks of cell failure by formation of electrode-spanning structures that internally short-circuit the cell. In comparison, Al electrodeposits on Au sheets to form evenly dispersed nanoparticles (**Figure 3b**). The average size by counting more than 200 particles is 237nm (**Figure S2**). It is known that the substrate with high surface area will dilute the real current density of electrode and contribute the uniform deposition, which is very straightforward for 3D current collectors. In our case, the Au nanosheet exhibits very high-aspect-ratio over 100 (10-20μm length or width, 90nm thickness).[47] This character proves that the electroactive area is still the surface of Au nanosheet, which is close to pure stainless steel. The SEM image also demonstrates that the Al is majorly deposited on the top surface of Au nanosheet, rather than under Au nanosheet. Therefore, the similar crystal structure between Al and Au as well as the exposing low surface energy (111) facet are supposed to be the major reason for uniform deposition.

Operando visualization experiments were designed to monitor the growth of Al on various substrates. The results show that non-planar, dendrite-like structures emerge in the SS case at a deposition capacity of 1mAh (**Figure 4a**). In comparison, formation of dendrite-like Al structures is clearly suppressed on the Au substrates at a deposition capacity of 2mAh, which is consistent with the SEM images (Figure 4b). It should be noticed that due to the high specific capacity of Al by volume, the theoretical thickness of Al is only about 2.5μm (2mAh), which makes it difficult to distinguish through optical microscopy.

Journal Name

ARTICLE

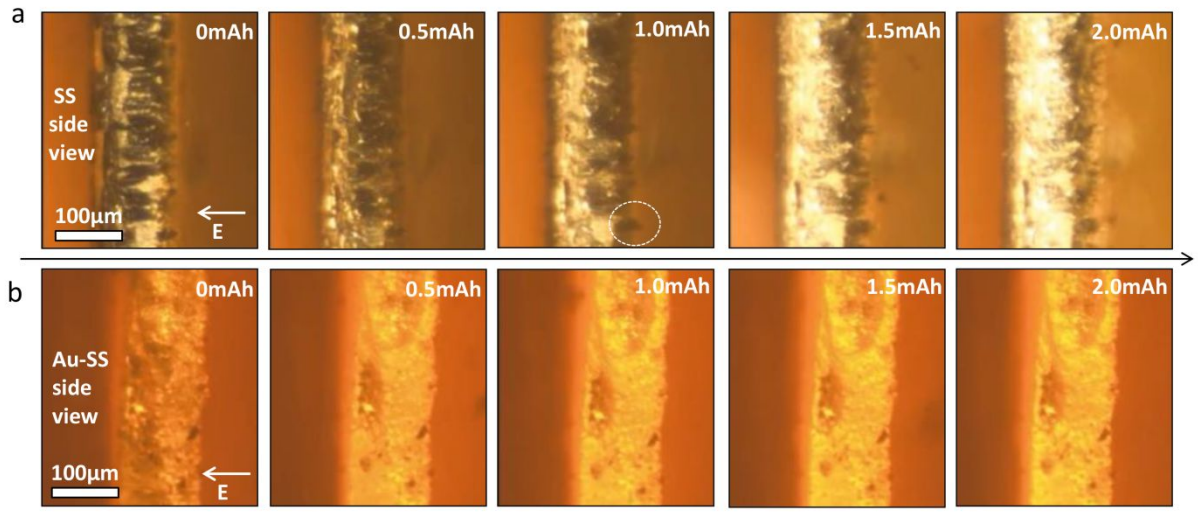

Fig. 4: In-situ investigations of electrodeposited Al on a) stainless steel and b) Au nanosheets. The current density is 15 mA/cm^2. The white dash lined circle of 1.0mAh in Figure 4a labels the dendrite like Al.

Galvanostatic discharge/charge experiments were performed to measure the efficiency of Al plating and stripping. Due to the uneven deposition of Al, the Coulombic efficiency (CE) of Al//SS electrochemical cells is highly variable. Additionally, the cells fail by short-circuiting at the 274th cycle (**Figure S3a**). As a comparison, when both Al and SS substrates are coated with the Au nanosheets, the stripping/plating profiles of the Au-Al//Au-SS electrochemical cells show narrow polarization and very high CE values, over 99% at 500th cycle (**Figure 5a-b**). At a high stripping/plating current density of 3mA/cm^2, the effect of Au coating is even larger. Whereas the Al//SS electrochemical cells fail by short-circuiting at around the 54th cycle (**Figure S3b**), the CE of Au-Al//Au-SS electrochemical cell maintains CE values of 98.9% after 150th cycles (**Figure 5c-d**). As a final rigorous experiment to evaluate the impacts of the Au coating, we created cells in which limited amounts of Al are employed. In particular, 10mAh/cm^2 Al is firstly deposit on Au, and the coated substrate used as the Al source (anode) in an Al-Au//Au-SS electrochemical cell. Due to the uniform deposition of Al on Au anode, the built cells again manifest high CE values of 98.8% at 80th cycle at a relatively high current density of 3mA/cm^2 and higher areal capacity of 0.5 mAh/cm^2 than literature (less than 0.2mAh/cm^2). [2,9,19,53] (**Figure 5e-f**).

Journal Name

ARTICLE

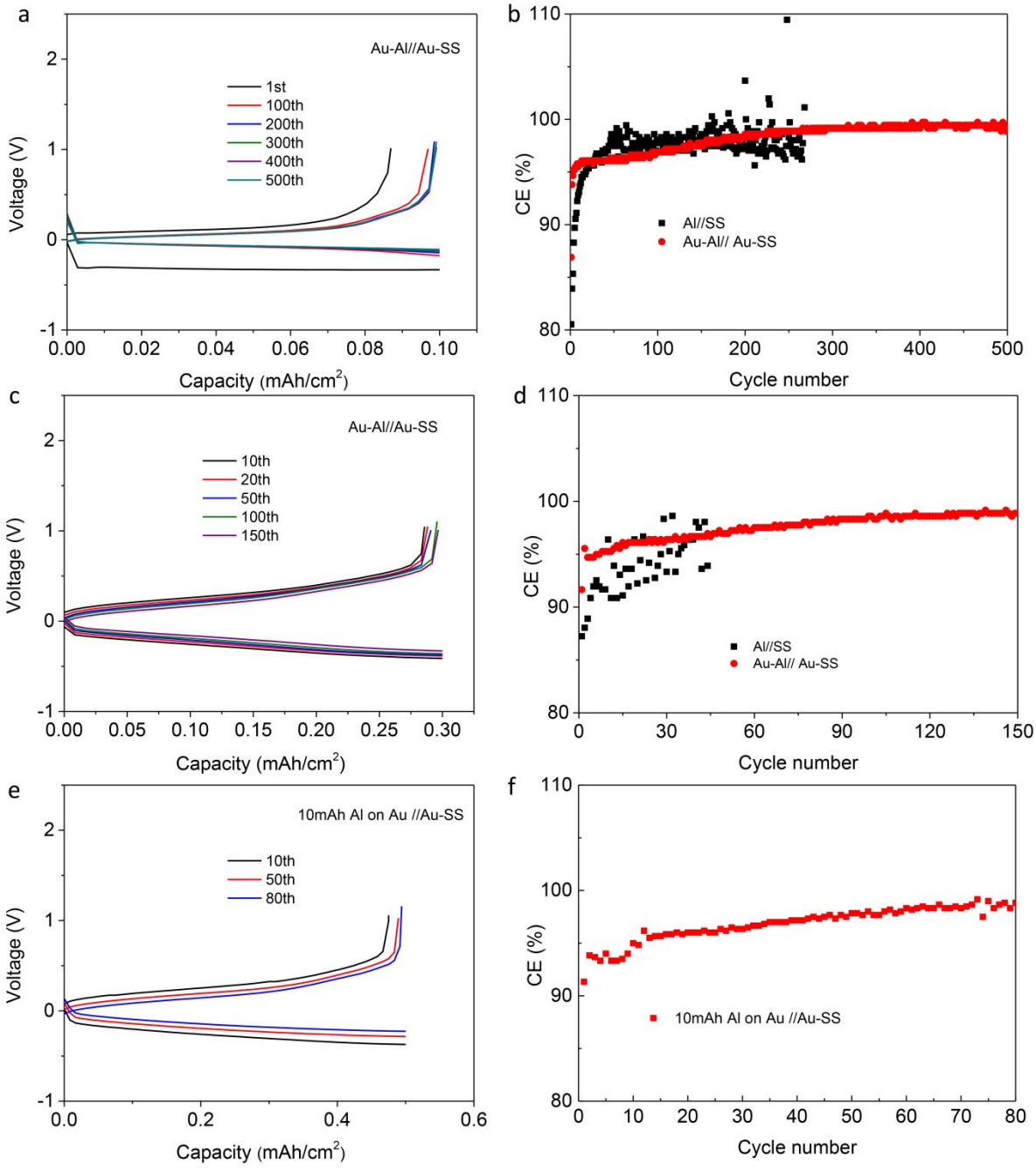

Figure 5: Aluminum stripping and plating performance in Al//SS electrochemical cells with or without Au protection. Al plating/stripping profiles of a, c) Au-Al//Au-SS electrochemical cells, and e) limited Al (10mAh) on Au//Au-SS electrochemical cells. b, d, f) Corresponding Coulombic efficiencies (CEs). The current density for a) and b) is 1mA/cm^2, c) and d) is 3mA/cm^2, e) and f) is 3mA/cm^2. The time of discharge is 6mins for a- d) and 10mins for e) and f)

The high CEs of Al stripping and plating encourage us to further evaluate the effects of substrates on Al in full-cell rechargeable batteries **(Figure S4)**. For this purpose, three types of cells, Al metal//Graphene (Al//G), stainless steel//Graphene (SS//G) and Au-coated stainless steel//Graphene (Au-SS//G) have been assembled and compared their cycling behaviors. A

single piece of glass fiber was used as separator in all of these battery cells. Due to the corrosion by the IL-based electrolytes, the SS//G cells exhibit very low CE values for first few cycles **(Figure 6a**). The charge/discharge profiles of the Au-SS//G (**Figure 6c, Figure S5**) cells are similar to those of the Al//G (**Figure 6b**) batteries, which benefits from the anti-corrosion of Au. After approximate 200 cycles, the CE values for both the SS//G and Al//G batteries are seen to fall sharply (**Figure 6d**), accompanied by a transition to a state where the cells appear to endlessly charge at a largely reduced voltage (**Figure S6**). The charging process corresponds to the deposition of Al (**Figure 1**), and thus the endless-charging phenomenon can be explained in terms of electrical connection of the two electrodes due to proliferation of non-planar Al electrodeposits. The results also demonstrate that Al metal is not a good substrate for Al deposition. As shown in Figure 2a, the commercial Al foil exposes both (111) and (200) (dominant) surface facet rather than (111) surface with lower surface energies; meaning that it is in fact not a good substrate for homoepitaxial deposition of Al. This finding is significant because it explains why several layers of separators are typically needed to support long-term cycling of Al electrodes reported in earlier studies.[6] Additionally, Al foil is covered by dense oxidation layer, which may not be removed homogeneously even in an IL-electrolyte. We believe that both factors combine to result in the uneven deposition of Al on Al foil. As comparisons, the Au-SS//G batteries show the stable galvanolstatic charge/discharge profiles (**Figure 6b**). Meanwhile, the polarization between discharge/charge is also smaller than Al//G and SS//G batteries (**Figure S7**). The Au-SS//G batteries retain the capacity of over 80% at 1000th cycles and over 74% at 2000th cycle with average CE of ~98% (**Figure 6d**). Therefore, using gold nanosheets as counter electrode instead of Al at least provide two advantages. 1) The reduced mass of counter electrode (1~2 mg/cm^2) due to the ultrathin structure of Au nanosheet compared with commercial Al foil (0.25mm thick, ~70mg/cm^2). 2) Even depositing on Al foil, the Al metal can still form dendrite-like structures, however, the Au nanosheet can regulate the growth of Al, which largely improves the cycling life of batteries.

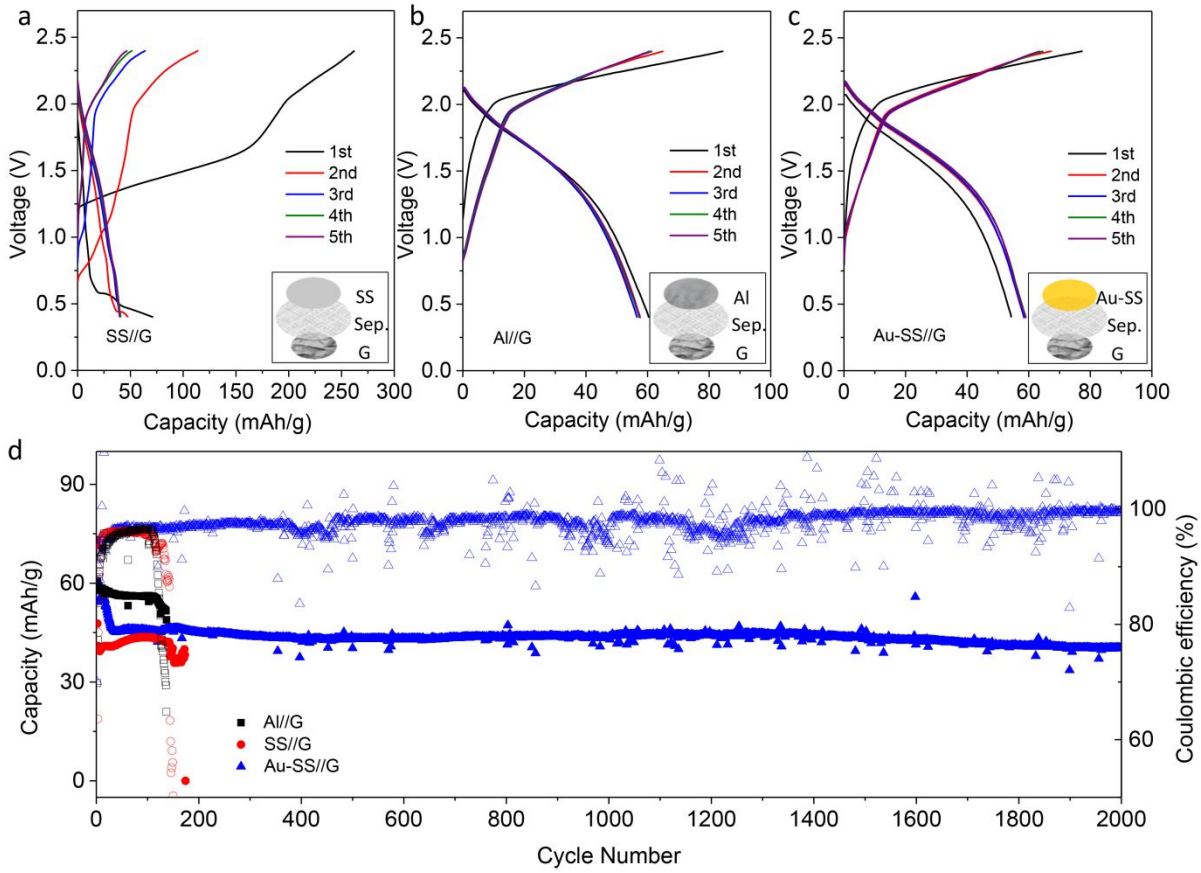

Fig. 6: Performance of dual-ion Al full batteries. Charge/discharge profiles of a) SS//Graphite (SS//G) batteries, b) Al//Graphene (Al//G) batteries, c) Au coated SS/Graphene (Au-SS//G) batteries at 1.4mA/cm^2. d) Corresponding cycling performance and CEs of three types of dual-ion batteries

Conclusions

In summary, through regulating the growth of Al by introducing the 2-D Au nanosheet, we successfully solve the problem of uneven deposition of Al metal. Further studies shows that the Au nanosheet leads to the high efficient Al plating and stripping with CEs of over 99% for 500 cycles. The built full batteries with

Au nanosheets anode and graphene cathode show long term stability over 2000 cycles. This work opens a new gate to rationally design the anode for dual-ion Al batteries. Other substrates that shares similar structures with Al, for example Ag, Pt and even Al itself with strong orientation of crystal facet can be designed as anode for Al based batteries.

Conflicts of interest

There are no conflicts to declare

Acknowledgements

This work was supported as part of the Center for Mesoscale Transport Properties, an Energy Frontier Research Center supported by the U.S. Department of Energy, Office of Science, Basic Energy Sciences, under award #DE-SC0012673. This work made use of the Cornell Center for Materials Research Shared Facilities which are supported through the NSF MRSEC program (DMR-1719875).

ORCID

Qing Zhao: 0000-0003-0625-9892

JingXu Zheng: 0000-0002-0673-0560

Yue Deng: 0000-0002-1683-5884

Lynden Archer: 0000-0001-9032-2772

Notes and references

1 M. S. Whittingham, *Chem. Rev.*, 2004, **104**, 4271-4301.
2 M. Armand and J. M. Tarascon, *Nature*, 2008, **451**, 652-657.
3 J. Muldoon, C. B. Bucur and T. Gregory, *Chem. Rev.*, 2014, **114**, 11683-11720.
4 G. A. Elia, K. Marquardt, K. Hoeppner, S. Fantini, R. Lin, E. Knipping, W. Peters, J. F. Drillet, S. Passerini and R. Hahn, *Adv Mater*, 2016, **28**, 7564-7579.
5 N. Jayaprakash, S. K. Das and L. A. Archer, *Chem. Commun.*, 2011, **47**, 12610-12612.
6 M. C. Lin, M. Gong, B. Lu, Y. Wu, D. Y. Wang, M. Guan, M. Angell, C. Chen, J. Yang, B. J. Hwang and H. Dai, *Nature*, 2015, **520**, 325-328.
7 H. Yang, H. Li, J. Li, Z. Sun, K. He, H. M. Cheng and F. Li, *Angew. Chem. Int. Ed.*, 2019, **58**, 11978-11996.
8 L. Xue, S. Xin, J. B. Goodenough and C. A. Angell, *ACS Energy Lett.*, 2017, **2**, 1534-1538.
9 W. I. Al Sadat and L. A. Archer, *Sci. Adv.*, 2016, **2**, e1600968.
10 Y. Zhang, S. Liu, Y. Ji, J. Ma and H. Yu, *Adv. Mater.*, 2018, **30**, e1706310.
11 Q. Zhao, M. J. Zachman, W. I. Al Sadat, J. Zheng, L. F. Kourkoutis and L. Archer, *Sci. Adv.*, 2018, **4**, eaau8131.
12 H. Wang, S. Gu, Y. Bai, S. Chen, F. Wu and C. Wu, *ACS Appl. Mater. Interfaces*, 2016, **8**, 27444-27448.
13 L. D. Reed, A. Arteaga and E. J. Menke, *J. Phys. Chem. B*, 2015, **119**, 12677-12681.
14 T. Mandai and P. Johansson, *J. Mater. Chem. A*, 2015, **3**, 12230-12239.
15 M. Chiku, S. Matsumura, H. Takeda, E. Higuchi and H. Inoue, *J. Electrochem. Soc.*, 2017, **164**, A1841-A1844.
16 Y. Nakayama, Y. Senda, H. Kawasaki, N. Koshitani, S. Hosoi, Y. Kudo, H. Morioka and M. Nagamine, *Phys. Chem. Chem. Phys.: PCCP*, 2015, **17**, 5758-5766.
17 A. A. Fannin, D. A. Floreani, L. A. King, J. S. Landers, B. J. Piersma, D. J. Stech, R. L. Vaughn, J. S. Wilkes and J. L. Williams, *J. Phys. Chem.*, 1984, **88**, 2614-2621.
18 Z. A. Zafar, S. Imtiaz, R. Razaq, S. Ji, T. Huang, Z. Zhang, Y. Huang and J. A. Anderson, *J. Mater. Chem. A*, 2017, **5**, 5646-5660.
19 H. Chen, H. Xu, S. Wang, T. Huang, J. Xi, S. Cai, F. Guo, Z. Xu, W. Gao and C. Gao, *Sci. Adv.* 2017, **3**, eaao7233.
20 Y. Wu, M. Gong, M. C. Lin, C. Yuan, M. Angell, L. Huang, D. Y. Wang, X. Zhang, J. Yang, B. J. Hwang and H. Dai, *Adv. Mater.*, 2016, **28**, 9218-9222.
21 C. Li, S. Dong, R. Tang, X. Ge, Z. Zhang, C. Wang, Y. Lu and L. Yin, *Energy Environ. Sci.* 2018, **11**, 3201-3211.
22 G. Cohn, L. Ma and L. A. Archer, *J. Power Sources*, 2015, **283**, 416-422.
23 Y. Hu, B. Luo, D. Ye, X. Zhu, M. Lyu and L. Wang, *Adv. Mater.*, 2017, **29**.
24 L. X. Geng, G. C. Lv, X. B. Xing and J. C. Guo, *Chem. Mater.*, 2015, **27**, 4926-4929.
25 T. Gao, X. Li, X. Wang, J. Hu, F. Han, X. Fan, L. Suo, A. J. Pearse, S. B. Lee, G. W. Rubloff, K. J. Gaskell, M. Noked and C. Wang, *Angew. Chem. Int. Ed.*, 2016, **55**, 9898-9901.
26 K. Liang, L. Ju, S. Koul, A. Kushima and Y. Yang, *Adv. Energy Mater.*, 2019, **9**, 1802543.
27 X. W. Yu and A. Manthiram, *Adv. Energy Mater.*, 2017, **7**, 1700561.
28 S. Zhang, X. Tan, Z. Meng, H. Tian, F. Xu and W.-Q. Han, *J. Mater. Chem. A*, 2018, **6**, 9984-9996.
29 X. F. Zhang, S. Q. Jiao, J. G. Tu, W. L. Song, X. Xiao, S. J. Li, M. Y. Wang, H. P. Lei, D. H. Tian, H. S. Chen and D. N. Fang, *Energy Environ. Sci.*, 2019, **12**, 1918-1927.
30 H. Wang, Y. Bai, S. Chen, X. Luo, C. Wu, F. Wu, J. Lu and K. Amine, *ACS Appl. Mater. Interfaces*, 2015, **7**, 80-84.
31 Q. Zhao, L. Liu, J. Yin, J. Zheng, D. Zhang, J. Chen and L. A. Archer, *Angew. Chem. Int. Ed.*, 2020, **59**, 3048-3052.
32 H. Wang, S. Gu, Y. Bai, S. Chen, N. Zhu, C. Wu and F. Wu, *J. Mater. Chem. A*, 2015, **3**, 22677-22686.
33 X. Wen, Y. Liu, A. Jadhav, J. Zhang, D. Borchardt, J. Shi, B. M. Wong, B. Sanyal, R. J. Messinger and J. Guo, *Chem. Mater.*, 2019, **31**, 7238-7247.
34 A. VahidMohammadi, A. Hadjikhani, S. Shahbazmohamadi and M. Beidaghi, *ACS Nano*, 2017, **11**, 11135-11144.
35 D. J. Kim, D.-J. Yoo, M. T. Otley, A. Prokofjevs, C. Pezzato, M. Owczarek, S. J. Lee, J. W. Choi and J. F. Stoddart, *Nature Energy*, 2018, **4**, 51-59.
36 S. Wang, S. Huang, M. Yao, Y. Zhang and Z. Niu, *Angew. Chem. Int. Ed.* 2020, **59**, 11800-11807.
37 K. V. Kravchyk, C. Seno and M. V. Kovalenko, *Acs Energy Lett.*, 2020, **5**, 545-549.
38 K. V. Kravchyk, S. Wang, L. Piveteau and M. V. Kovalenko, *Chem. Mater.*, 2017, **29**, 4484-4492.
39 X. L. Zhang, Y. B. Tang, F. Zhang and C. S. Lee, *Adv. Energy Mater.*, 2016, **6**, 1502588.
40 Q. Liu, H. Wang, C. Jiang and Y. Tang, *Energy Storage Mater.*, 2019, **23**, 566-586
41 J. W. Matthews, Epitaxial Growth (Ed: J. W. Matthews) *Academic, NewYork*, 1975.
42 J. Zheng, Q. Zhao, T. Tang, J. Yin, C. D. Quilty, G. D. Renderos, X. Liu, Y. Deng, L. Wang, D. C. Bock, C. Jaye, D. Zhang, E. S. Takeuchi, K. J. Takeuchi, A. C. Marschilok and L. A. Archer, *Science*, 2019, **366**, 645-648.
43 J. Y. Shi, J. Zhang and J. Guo, *Acs Energy Lett.*, 2019, **4**, 2124-2129.
44 L. D. Reed and E. Menke, *J. Electrochem. Soc.*, 2013, **160**, A915-A917.
45 J. Gong, *Chem. Rev.*, 2012, **112**, 2987-3054.
46 G. D. Moon, G. H. Lim, J. H. Song, M. Shin, T. Yu, B. Lim and U. Jeong, *Adv. Mater.*, 2013, **25**, 2707-2712.

47 C. C. Li, W. P. Cai, B. Q. Cao, F. Q. Sun, Y. Li, C. X. Kan and L. D. Zhang, *Adv. Funct. Mater.*, 2006, **16**, 83-90.
48 K. S. Nagy, S. Kazemiabnavi, K. Thornton and D. J. Siegel, *ACS Appl. Mater. Interfaces*, 2019, **11**, 7954-7964.
49 R. L. Perry, K. M. Jones, W. D. Scott, Q. Liao and C. L. Hussey, *J. Chem. Engineering Data*, 1995, **40**, 615-619
50 T. Jiang, M. J. Chollier Brym, G. Dubé, A. Lasia and G. M. Brisard, *Surf. Coatings Technology*, 2006, **201**, 1-9
51 A. Nyman, M. Behm and G. Lindbergh, *Electrochimica Acta*, 2008, **53**, 6356-6365
52 Q. Zhao, Z. Tu, S. Wei, K. Zhang, S. Choudhury, X. Liu and L. A. Archer, *Angew. Chem. Int. Ed.*, 2018, **57**, 992-996.
53 E. J. Zhang, J. Wang, B. Wang, X. Z. Yu, H. G. Yang and B. G. Lu, *Energy Storage Mater.*, 2019, **23**, 72-78

Journal Name

ARTICLE

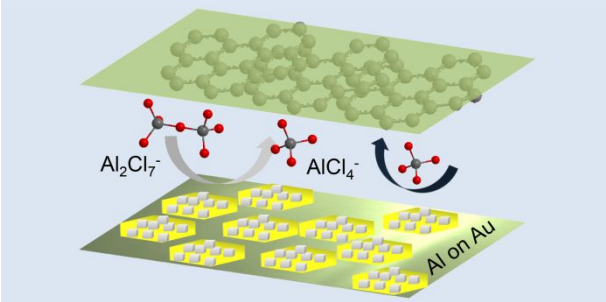

TOC

2-D Au coatings enable stable and uniform deposition of Aluminum.